High-precision quantum dynamics of He₂ over the b $^3\Pi_g$ -c $^3\Sigma_q^+$ electronic subspace by including non-adiabatic, relativistic, and QED corrections and couplings @

Cite as: J. Chem. Phys. 163, 081102 (2025); doi: 10.1063/5.0288277 Submitted: 30 June 2025 · Accepted: 31 July 2025 ·







Published Online: 22 August 2025

Balázs Rácsai, D Péter Jeszenszki, D Ádám Margócsy, D and Edit Mátyus D





AFFILIATIONS

MTA-ELTE "Momentum" Molecular Quantum electro-Dynamics Research Group, Institute of Chemistry, Eötvös Loránd University, Pázmány Péter sétány 1/A, Budapest H-1117, Hungary

a) Author to whom correspondence should be addressed: edit.matyus@ttk.elte.hu

ABSTRACT

Relativistic, quantum electrodynamics, and non-adiabatic corrections and couplings are computed for the b $^3\Pi_g$ and c $^3\Sigma_g^+$ electronic states of the helium dimer. The underlying Born-Oppenheimer potential energy curves are converged to 1 ppm (1:10⁶) relative precision using a variational explicitly correlated Gaussian approach. The quantum nuclear motion is computed over the b $^3\Pi_g$ -c $^3\Sigma_g^+$ (and B $^1\Pi_g$ -C $^1\Sigma_g^+$) 9-(12-)dimensional electronic-spin subspace coupled by non-adiabatic and relativistic (magnetic) interactions. The electron's anomalous magnetic moment is also included; its effect is expected to be visible in high-resolution experiments. The computed rovibronic energy intervals are in excellent agreement with the available high-resolution spectroscopy data, including the rovibronic b ${}^3\Pi_g$ -state fine structure. Finestructure splittings are also predicted for the c $^3\Sigma_g^+$ levels, which have not been fully resolved experimentally, yet.

Published under an exclusive license by AIP Publishing. https://doi.org/10.1063/5.0288277

This work focuses on the electronically excited states of the triplet helium dimer, which, in contrast to the very weakly bound singlet helium dimer ground state, possesses a rich rovibronic level structure with intriguing magnetic properties. Triplet helium dimer states have recently attracted experimental attention for generating cold molecules and using them in precision tests of quantum electrodynamics.²⁻⁵ So far, the a ${}^{3}\Sigma_{\rm u}^{+}$ state of He₂ has been used to generate He₂⁺ rovibrational states for precision spectroscopy measurements.⁶⁻⁸ He₂⁺ is a small calculable molecular system 9-12 and, thus, an ideal target for precision physics. In comparison with the H₂ molecule, another precision spectroscopy prototype, 13-16 the magnetic properties of the helium dimer (and its cation) can potentially offer a combination of versatile experimental tools and techniques for cooling, quantum state preparation, and measurement. Furthermore, the electronically excited helium dimer states have recently been linked to plasma kinetics.¹⁷ In addition to ongoing experimental work,²⁻⁵ old experimental data

on the electronic-vibrational-rotational level structure and even fine-structure splittings of some transitions are available, e.g., Refs. 18-28, which have remained largely unexplained by ab initio molecular quantum theory to date. It may be orienting to mention that the a ${}^{3}\Sigma_{\rm u}^{+}$ state of the He₂ Rydberg molecule is the 2s state, and b ${}^{3}\Pi_{g}$ and c ${}^{3}\Sigma_{g}^{+}$ are the closest-lying gerade states, corresponding to p character.

Early theoretical and computational work includes studies by valence bond theory computations. 29-31 Then, the multiconfigurational self-consistent field (MCSCF) approach, with special, augmented basis sets, was used, 32-36 although the results lag behind even the old experimental data. More recent computational work employed the Multireference Configuration Interaction (MRCI) method,³⁷ the equation-of-motion coupled cluster method,³⁸ MRCI combined with neural networks, ¹⁷ and the R-matrix method. ³⁹ Furthermore, there is a single variational explicitly correlated Gaussian (ECG) computation,⁴⁰ which has been the most accurate so far. Despite all these efforts, a considerable gap still exists between theory and experiment for this simple Rydberg molecule, which is the smallest excimer.

This work, part of a series of variational explicitly correlated Gaussian computations carried out by our group, 12,41,42 aims to provide computational results sufficiently accurate to guide, help interpret, and perhaps even challenge modern experiments on this molecular physics prototype.

For direct comparison with experimental spectroscopy transitions and energy intervals, we start out from the non-relativistic molecular Schrödinger equation

$$\hat{H}\Psi(\mathbf{r},\boldsymbol{\rho}) = E\Psi(\mathbf{r},\boldsymbol{\rho}),\tag{1}$$

with the translationally invariant Hamiltonian

$$\hat{H} = -\frac{1}{2\mu} \Delta_{\rho} + \hat{H}_{e} - \frac{1}{8\mu} \hat{P}_{e}^{2}, \tag{2}$$

where $\mu = M_{\rm nuc}/2$ is the reduced mass, $\rho = R_1 - R_2$ is the internuclear position vector, and $\hat{P}^e = -i\sum_{i=1}^{n_e} \nabla_{r_i}$ is the total (linear) momentum of the n_e electrons. \hat{H}^e is the electronic Hamiltonian, for which we (numerically) solve the Schrödinger equation

$$\hat{H}^{e}\varphi_{n} = U_{n}\varphi_{n} \tag{3}$$

(with $\langle \varphi_{n'} | \varphi_n \rangle = \delta_{n'n}$) to obtain the φ_n electronic states relevant for the experiments. We perform the electronic structure computations in the body-fixed (BF) frame in which the ρ internuclear vector defines the z axis. The electronic state is characterized by its total spin, $\hat{S}^2 \varphi_n = S(S+1)\varphi_n$, and the z BF axis is the quantization axis for

the orbital and spin angular momenta of the electrons, $\hat{L}_z \varphi_n = \Lambda \varphi_n$ and $\hat{S}_z \varphi_n = \Sigma \varphi_n$.

In order to numerically solve the Schrödinger equation of the molecular Hamiltonian, Eqs. (1) and (2), we write the molecular wave function as a linear combination of products of electronic, rotational, and vibrational functions,

$$\Psi(\mathbf{r},\boldsymbol{\rho}) = \sum_{n \in N} \sum_{D}^{J} \sum_{C=-I} \sum_{k} c_{n,k}^{\Omega} \varphi_{n}(\mathbf{r},\boldsymbol{\rho}) \tilde{D}_{M_{J}\Omega}^{J}(\theta,\phi,\chi) \frac{1}{\rho} g_{k}(\rho), \quad (4)$$

where $n = (l, S, \Lambda, \Sigma)$ collects the relevant electronic state labels and quantum numbers and it is summed over all electronic states included in the \mathcal{P} "active" subspace (for which the indices are collected in the set N_P). $g_k(\rho)$ are the vibrational basis functions. The (normalized) $\tilde{D}'_{M_1\Omega}(\theta,\phi,\chi)$ Wigner D matrices describe the rotation of the body-fixed frame (x, y, z) (rotating diatom with BF spin and orbital angular momenta) with respect to the laboratory-fixed system (X, Y, Z), where the $\Omega = \Lambda + \Sigma$ and M_I quantum numbers denote the projection of the total rotational plus electronic angular momentum onto the z and Z axes, respectively, $\hat{J}_z \tilde{D}'_{M_I \Omega} = \Omega \tilde{D}'_{M_I \Omega}$, $\hat{J}_Z \tilde{D}^J_{M_J \Omega} = M_J \tilde{D}^J_{M_J \Omega}$, and $\hat{J}^2 \tilde{D}^J_{M_J \Omega} = J(J+1) \tilde{D}^J_{M_J \Omega}$. The \hat{J} total angular momentum operator acts on the (θ, ϕ, χ) Euler angles of the Wigner D matrices, while the \hat{S} and \hat{L} operators act on the electronic spin and spatial degrees of freedom. The helium-4 nuclei have zero spin, so the nuclear spin angular momentum is considered only for the spin statistics (of bosonic nuclei).

We insert the ansatz of Eq. (4) into Eq. (1), multiply both sides from the left by the product of an electronic and a Wigner D element, and integrate for the electronic coordinates and the Euler angles to arrive at the following coupled radial (vibrational) equation:

$$E\sum_{k} c_{n',k}^{\Omega'} \frac{1}{\rho} g_{k} = \sum_{n \in N_{D}} \sum_{\Omega=-I}^{J} \sum_{k} c_{n,k}^{\Omega} \left(\varphi_{n'} \tilde{D}_{M_{J}\Omega'}^{J} \right) - \frac{1}{2\mu} \Delta_{\rho} + \hat{H}_{e} - \frac{1}{8\mu} \hat{P}_{e}^{2} |\varphi_{n} \tilde{D}_{M_{J}\Omega}^{J} \rangle \frac{1}{\rho} g_{k}. \tag{5}$$

For practical computations, we rewrite the nuclear Laplacian using the \hat{R} rotational angular momentum operator as

$$\Delta_{\rho} = \frac{1}{\rho^{2}} \frac{\partial}{\partial \rho} \left(\rho^{2} \frac{\partial}{\partial \rho} \right) - \frac{1}{\rho^{2}} \hat{\mathbf{R}}^{2}
= \frac{1}{\rho^{2}} \frac{\partial}{\partial \rho} \left(\rho^{2} \frac{\partial}{\partial \rho} \right) - \frac{1}{\rho^{2}} \left[(\hat{J}^{2} - \hat{J}_{z}^{2}) + (\hat{L}_{x}^{2} + \hat{L}_{y}^{2}) + (\hat{S}^{2} - \hat{S}_{z}^{2}) \right]
- (\hat{J}^{+} \hat{S}^{-} + \hat{J}^{-} \hat{S}^{+}) - (\hat{J}^{+} \hat{L}^{-} + \hat{J}^{-} \hat{L}^{+}) + (\hat{S}^{+} \hat{L}^{-} + \hat{S}^{-} \hat{L}^{+}) \right]. (6)$$

The $\hat{O}^{\pm} = \hat{O}_x \pm i\hat{O}_y$ body-fixed ladder operator matrix elements are calculated according to established relations⁴³ $\langle D_{M_{I}\Omega'}^{J}|\hat{J}^{\pm}D_{M_{I}\Omega}^{J}\rangle = \delta_{\Omega',\Omega\mp 1}C_{I\Omega}^{\mp}, \quad \langle \varphi_{n'}|\hat{S}^{\pm}\varphi_{n}\rangle = \delta_{\Sigma',\Sigma\pm 1}C_{S\Sigma}^{\pm}$ with $C_{AB}^{\pm} = \left[A(A+1) - B(B\pm 1)\right]^{1/2}$. The orbital angular momentum integrals for the electronic states of molecules are computed numerically, $\langle \varphi_{n'} | \hat{L}^{\pm} \varphi_n \rangle = \delta_{\Lambda', \Lambda \pm 1} \langle \varphi_{n'} | [\hat{L}_x \pm i \hat{L}_y] \varphi_n \rangle$. For computational feasibility, we explicitly include only the qualitatively important electronic states in the \mathcal{P} subspace. However, for rovibronic computations of spectroscopic accuracy, it is necessary to account for the remaining (small) effect of the (1 - P) electronic Hilbert space. By perturbation theory (contact transformation), this leads to the following correction^{44,45} to the right-hand side of Eq. (5):

$$\frac{1}{2\mu^2} \sum_{n} \sum_{\Omega} \langle \tilde{D}_{M_j\Omega'}^{J} | \nabla_{\tilde{\rho}} \cdot \langle \nabla_{\tilde{\rho}} \varphi_{n'} | \hat{\mathcal{R}} | \nabla_{\rho} \varphi_n \rangle \nabla_{\rho} \cdot | \tilde{D}_{M_j\Omega}^{J} \rangle, \tag{7}$$

where $\bar{\rho} = \rho = R_1 - R_2$ was introduced only to help label the corresponding factors of the two scalar products unambiguously. The correction contains the reduced resolvent of the electronic Hamiltonian,

$$2\hat{\mathcal{R}} = \hat{\mathcal{R}}_{n'} + \hat{\mathcal{R}}_n = \left[(\hat{H}_e - E_{n'})^{-1} + (\hat{H}_e - E_n)^{-1} \right] P^{\perp}, \quad (8)$$

where $P^{\perp}=1-\sum_{n\in\mathcal{P}}|\varphi_n\rangle\langle\varphi_n|$ projects out the electronic states explicitly coupled in Eq. (4). For the c $^3\Sigma_{\rm g}^+$ electronic state with $\Lambda = 0$, Eq. (7) leads to the following contributions to the reduced rotational (x = r) and vibrational (x = v) masses:

$$\frac{1}{\mu_n^{\rm x}(\rho)} = \frac{1}{\mu} \left[1 - \frac{\delta m_n^{\rm x}(\rho)}{\mu} \right] \approx \frac{1}{\mu + \delta m_n^{\rm x}(\rho)} \tag{9}$$

with

$$\delta m_n^{\mathrm{x}}(\rho) = \left(\frac{\partial \varphi_n}{\partial \rho_{a_{\mathrm{x}}}} | (\hat{H}_{\mathrm{e}} - E_n)^{-1} P^{\perp} | \frac{\partial \varphi_n}{\partial \rho_{a_{\mathrm{x}}}} \right), \tag{10}$$

where $a_x = z$ for x = v and $a_x = x/y$ for x = r. We note that the vibrational non-adiabatic mass (perturbatively) accounts for all homogeneous ($\Delta\Lambda = 0$) non-adiabatic couplings of the state with all other states of the same spatial symmetry (not explicitly, variationally coupled in the rovibronic treatment). The rotational mass accounts for the heterogeneous coupling ($\Delta\Lambda = \pm 1$) for all states not explicitly coupled within the variational treatment. It is important to note that only the effect of distant (non-crossing, separated by a finite gap⁴⁴) states can be accounted for in this manner; crossing or closelying electronic states must be coupled variationally (as the c and b states in the present system). Numerical illustrations for electronically excited hydrogenic states and vibronic states over coupled subspaces have been reported in Refs. 46 and 45. The b-state vibrational mass correction was also computed using Eq. (10). At the same time, the b-state rotational mass and further contributions

from the b-c coupling through the kinetic energy correction term, Eq. (7), are neglected here and left for future work (for technical reasons).

In the rovibronic Schrödinger equation, Eq. (5), we correct the electronic energy (PEC) with spin-independent (sn) and spin-dependent (sd) relativistic and QED corrections and couplings by adding the terms (α labeling here the fine-structure constant),

$$\alpha^{2} \langle \varphi_{n'} | \hat{H}_{\text{sn}}^{(2)} + \hat{H}_{\text{sd}}^{(2)} | \varphi_{n} \rangle + \alpha^{3} [E_{\text{sn}, \varphi_{n'}, \varphi_{n}}^{(3)} + \langle \varphi_{n'} | \hat{H}_{\text{sd}}^{(3)} | \varphi_{n} \rangle]. \tag{11}$$

The spin-independent corrections are, in short, the centroid relativistic (QED) energy corrections, whereas the spin-dependent corrections can be understood as the terms responsible for magnetic (dipolar and contact) interactions. The relativistic and QED corrections are computed in the non-relativistic quantum electrodynamics (nrQED) framework; the detailed expressions are reiterated in the supplementary material. For further details regarding the electron-spin (Σ) dependent terms, please see also Refs. 41 and 42; the centroid relativistic corrections are evaluated according to Ref. 47.

All in all, we arrive at the final form of the coupled radial equation,

$$\begin{split} E \sum_{k} c_{n',k}^{\Omega'} g_{k} &= \sum_{n \in N_{\mathcal{P}}} \sum_{\Omega = -J}^{J} \sum_{k} c_{n,k}^{\Omega} \left\{ \delta_{\Lambda'\Lambda} \delta_{\Sigma'\Sigma} \left[-\frac{\mathrm{d}}{\mathrm{d}\rho} \frac{1}{2\mu_{n}^{\mathrm{r}}} \frac{\mathrm{d}}{\mathrm{d}\rho} + \frac{J(J+1) - \Omega^{2}}{2\mu_{n}^{\mathrm{r}}\rho^{2}} + \frac{S(S+1) - \Sigma^{2}}{2\mu_{n}^{\mathrm{r}}\rho^{2}} + W_{n} \right] \\ &- \frac{1}{2\mu_{n}^{\mathrm{r}}\rho^{2}} \left[\delta_{\Lambda'\Lambda} \delta_{\Sigma'\Sigma\pm1} C_{J\Omega}^{\pm} C_{S\Sigma}^{\pm} + \delta_{\Lambda'\Lambda\pm1} \delta_{\Sigma'\Sigma} C_{J\Omega}^{\pm} \langle \varphi_{n'} | \hat{L}^{\pm} \varphi_{n} \rangle \right] \\ &+ \frac{1}{2\mu_{n}^{\mathrm{r}}\rho^{2}} \delta_{\Lambda'\Lambda\pm1} \delta_{\Sigma'\Sigma\pm1} C_{S\Sigma}^{\pm} \langle \varphi_{n'} | \hat{L}^{\pm} \varphi_{n} \rangle + \alpha^{2} \langle \varphi_{n'} | \hat{H}^{(2)} | \varphi_{n} \rangle + \alpha^{3} \left[E_{sn,\varphi_{n'},\varphi_{n}}^{(3)} + E_{sd,\varphi_{n'},\varphi_{n}}^{(3)} \right] \right\} g_{k}, \end{split} \tag{12}$$

where the BO potential energy curve with the diagonal Born–Oppenheimer (DBOC) or adiabatic correction is

$$W_{n} = U_{n} - \frac{1}{8\mu} \langle \varphi_{n} | \hat{P}_{e}^{2} \varphi_{n} \rangle - \frac{1}{2\mu} \langle \varphi_{n} | \frac{\partial^{2}}{\partial \rho^{2}} \varphi_{n} \rangle + \frac{1}{2\mu \rho^{2}} \langle \varphi_{n} | \hat{L}_{x}^{2} + \hat{L}_{y}^{2} | \varphi_{n} \rangle.$$

$$(13)$$

We neglected the effect of the non-adiabatic contact transformation on the relativistic and QED terms, and vice versa, the Foldy–Wouthuysen transformation on the nuclear motion operators. The corresponding terms would account for the combined relativistic, QED, and non-adiabatic coupling, and their consideration is left for future work.

Furthermore, we note that for the smallness of the magnetic splittings, we also performed computations without considering couplings due to the electron spin. In this case, it is convenient to use the total "spatial" angular momentum, $\hat{N} = \hat{R} + \hat{L}$, and then, we use the Wigner $\hat{D}_{M_N\Lambda}^N$ matrices to describe the spatial rotation of the diatom with orbital angular momentum in the BF frame, $\hat{N}_z \hat{D}_{M_N\Lambda}^N = \Lambda \hat{D}_{M_N\Lambda}^N$, $\hat{N}_Z \tilde{D}_{M_N\Lambda}^N = M_N \tilde{D}_{M_N\Lambda}^N$, and $\hat{N}^2 \tilde{D}_{M_N\Lambda}^N = N(N+1) \tilde{D}_{M_N\Lambda}^N$. Then, the coupled radial equation simplifies to

$$\begin{split} E \sum_{k} c_{n',k}^{\Lambda'} g_{k} &= \sum_{n \in N_{\mathcal{P}}} \sum_{\Lambda = -N}^{N} \sum_{k} c_{n,k}^{\Lambda} \\ &\times \left\{ \delta_{\Lambda'\Lambda} \left[-\frac{\partial}{\partial \rho} \frac{1}{2\mu_{n}^{V}} \frac{\partial}{\partial \rho} + \frac{N(N+1) - \Lambda^{2}}{2\mu_{n}^{r} \rho^{2}} + W_{n} \right] \right. \\ &\left. - \frac{1}{2\mu_{n}^{r} \rho^{2}} \delta_{\Lambda'\Lambda \pm 1} C_{N\Lambda}^{\pm} \langle \varphi_{n'} | \hat{L}^{\pm} \varphi_{n} \rangle \right. \\ &\left. + \alpha^{2} \langle \varphi_{n'} | \hat{H}^{(2)} | \varphi_{n} \rangle + \alpha^{3} E_{\text{sn}, \varphi_{n'}, \varphi_{n}}^{(3)} \right\} g_{k}. \end{split} \tag{14}$$

For rovibrational computations on a single electronic state, we solve the radial equation of Refs. 12 and 41 without and with considering fine-structure (zero-field splitting) effects, respectively.

The outlined theoretical framework (with further details in the supplementary material) benefited from reading several pioneering spectroscopy and *ab initio* studies. Most importantly, we mention the DUO program documentation⁴⁸ about a modern formalism using *ab initio* computations for astrophysical applications of diatomic molecules including non-adiabatic and spindependent couplings. We have also studied the series of work on the non-adiabatic couplings in the electronically excited states of the

hydrogen molecule by Dressler, Wolniewicz, and co-workers^{49,50} and even the early work of Kołos and Wolniewicz.⁵¹ The book by Lefebvre-Brion and Field⁴³ and the book by Brown and Carrington⁵² served as rich sources of ideas and information.

The J and N radial equations, Eqs. (12) and (14), are used with the PECs and correction and coupling curves evaluated numerically at a series of nuclear geometries (and then interpolated through the points). These quantities are shown in Fig. 1; they were computed numerically with the in-house developed computer program, QUANTEN, and are briefly explained in the following paragraphs. First, we solved the electronic Schrödinger equation, Eq. (3), in a non-linear variational procedure. The electronic wave function is written as a linear combination of anti-symmetrized products of $f(r; A_i, s_i)$ floating explicitly correlated Gaussian (fECG) functions and χ spin functions,

$$\varphi_n(\mathbf{r}) = \sum_{i=1}^{N_b} d_i \hat{\mathcal{P}}_G \hat{\mathcal{A}}_S \{ f(\mathbf{r}; \mathbf{A}_i, \mathbf{s}_i) \chi_{(S,\Sigma)}(\boldsymbol{\theta}_i) \},$$
(15)

$$f(\mathbf{r}; \mathbf{A}_i, \mathbf{s}_i) = \exp\left[\left(\mathbf{r} - \mathbf{s}_i\right)^{\mathrm{T}} \underline{\mathbf{A}}_i \left(\mathbf{r} - \mathbf{s}_i\right)\right],$$
 (16)

where the $\underline{A}_i = A_i \otimes I_3$ matrix is a real, symmetric, positive definite matrix with the $I_3 \in \mathbb{R}^{3 \times 3}$ unit matrix and the $A_i \in \mathbb{R}^{n_c \times n_c}$ matrix; $s_i \in \mathbb{R}^{3n_c}$ is a shift vector corresponding to the center of the fECG function. $\chi_{(S,\Sigma)}(\theta_i)$ is an electronic spin function constructed according to Refs. 41 and 42. The A_i , s_i , and θ_i parameters were generated according to the stochastic variational method 53,54 and refined with the Powell approach. 55 The \hat{A}_S electronic anti-symmetrization operator ensures fulfillment of the Pauli principle for the electronic part, while $\hat{\mathcal{P}}_G$ projects onto the selected irreducible representation (irrep) of the $D_{\infty h}$ point group.

In this work, we computed the c $^3\Sigma_g^+$ and the b $^3\Pi_g$ (x component in the Cartesian representation) electronic states of the helium dimer. First, fECG basis functions were generated and optimized (Table S1) at $\rho=2$ bohrs. Convergence tests and comparisons with standard electronic structure computations are collected in the supplementary material. Based on these tests, the basis sets used for the b and c electronic energies were converged to 3–5 cm⁻¹ (as an upper bound to the exact value) at $\rho=2$ bohrs.

The BO PECs for the b and c electronic states were generated by small consecutive displacements of ρ followed by rescaling

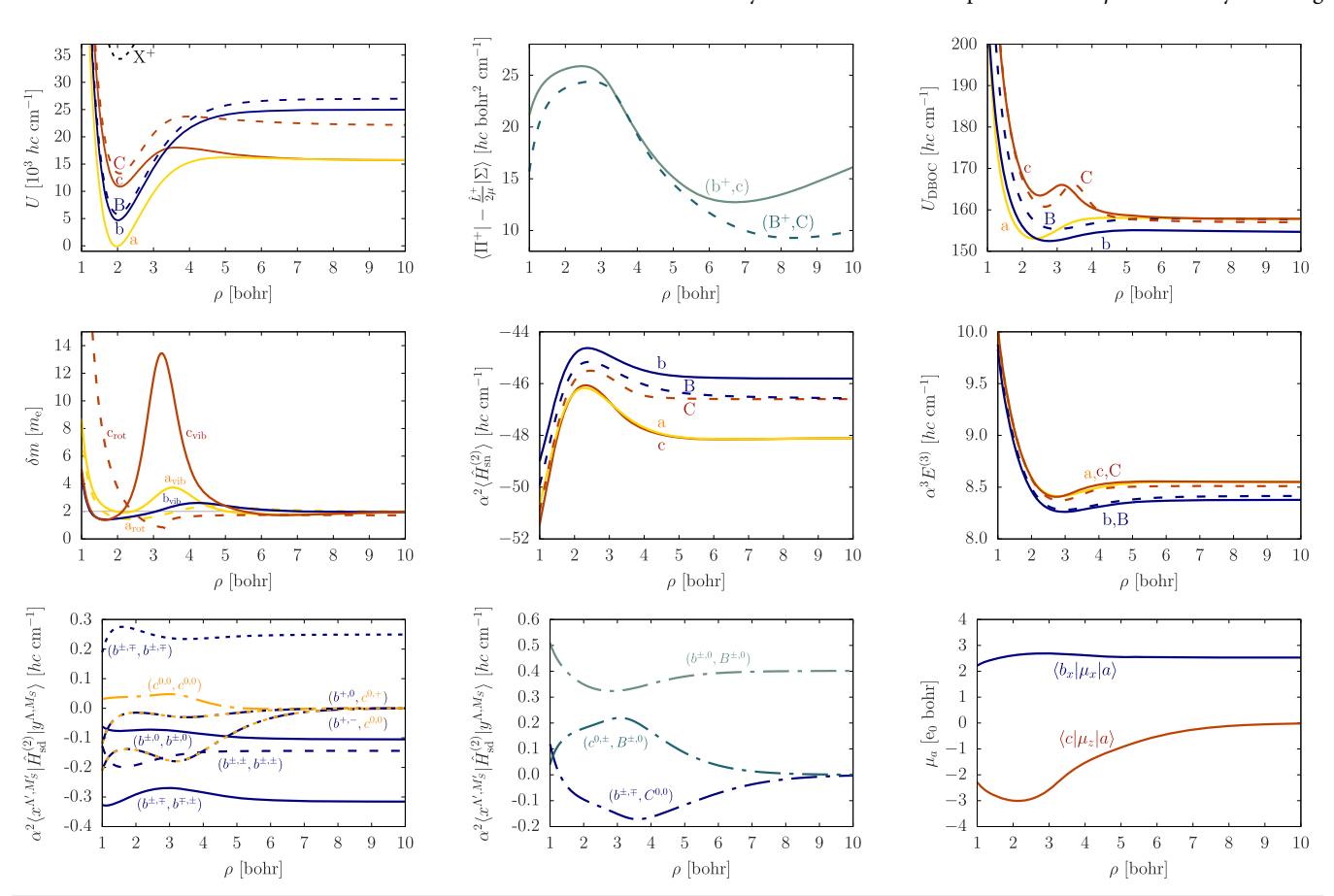


FIG. 1. He₂ b, c, B, and C electronic states: BO PEC, non-adiabatic coupling, DBOC correction, vibrational and rotational non-adiabatic mass correction, and leading-order relativistic and QED correction curves computed in this work. The a-state results are reproduced from Ref. 41, and the bottom of the X^{+} $^{2}\Sigma_{u}^{+}$ BO PEC of He₂ $^{+}$ 12 is plotted for comparison. The spin-dependent relativistic corrections and couplings (\hat{H}_{sd}) for the b, c, B, and C electronic states are also shown, computed in Ref. 42. All non-vanishing, non-adiabatic, and relativistic QED couplings, computed as part of Ref. 42, are plotted (see also Tables S6 and S7). The electric dipole (μ_{a}) transition moments connecting the b and c states with the a state, computed in this work, are also shown.

the s_i vectors and full reoptimization (in repeated Powell cycles) of all non-linear basis parameters. 11,46,56,57 This PEC generation procedure was started from $\rho = 2$ bohrs with a ± 0.1 bohr step size over the [1,10] bohr interval. This consecutive rescaling-refining procedure allowed us to approximately conserve the absolute error along a series of neighboring nuclear configurations, and thus, the relative properties (here, rovibrational excitation energies) are expected to be (1-2 orders of magnitude) more precise than the absolute electronic energies. Along the PECs, the electronic wave functions obtained from the variational fECG procedure were used to compute corrections and couplings.

Regarding the DBOC and non-adiabatic mass corrections, the $\langle \frac{\partial \varphi_{n'}}{\partial \rho} | \frac{\partial \widetilde{\varphi}_{n'}}{\partial \rho} \rangle$ and $\langle \varphi_{n'} | \frac{\partial \varphi_n}{\partial \rho} \rangle$ integrals were computed by finite differences, in which the optimized s_i fECG centers were rescaled in proportion to the (tiny) $\rho \pm \delta \rho$ variation. The electronic orbital angular momentum operators $\langle \varphi_{n'} | \hat{L}_a \varphi_n \rangle$ and $\langle \varphi_{n'} | \hat{L}_a^2 \varphi_n \rangle$ (a = x, y)were computed using the analytic integrals in QUANTEN. Auxiliary basis sets for the non-adiabatic vibrational and rotational mass corrections, Eq. (10), were optimized by minimization of the target quantities using the procedure of Ref. 45.

Regarding the relativistic (spin-independent, centroid) corrections, we employed the numerical Drachmanization approach described in Ref. 47 (Table S3 presents convergence tests). The QED (centroid) corrections were calculated using the regularized Dirac delta expectation values already computed for the relativistic corrections, and the Araki-Sucher (AS) term was computed with the integral transformation technique^{58,59} for the c state (and this AS curve was used also for the b, B, and C states; see the supplementary material). For the Bethe logarithm, we use the ioncore approximation and the values of the ground electronic state of $He_2^{3+}.^1$

The computation of spin-dependent relativistic couplings with fECG functions has recently been implemented in QUANTEN. The methodology is reported in a separate paper, 42 including extensive convergence tests for the b- and c-state couplings. The leading-order QED corrections to the spin-dependent couplings are due to the electron's anomalous magnetic moment, which is also accounted for; the technical and computational details are in Refs. 41 and 42. We had to pay attention to the phase of the electronic wave function; it was fixed for the computation of all (non-adiabatic, relativistic, and QED) couplings, and the phase of the (real-valued) electronic wave functions at neighboring PEC points was chosen so that their overlap is closer to +1, than to -1. For future computations (and to aid the experimental work), the electric dipole transition moments to the a ${}^3\bar{\Sigma}^+_u$ state were also computed as a function of the ρ internuclear distance and are shown in Fig. 1. The total computing time used to prepare this paper (including electronic structure optimization and all corrections and couplings, partly reported in Ref. 42) is estimated to be 150 kCPU hours.

QUANTEN uses the Cartesian representation of the basis and wave functions labeled as $\varphi_n^{a,\Sigma}$ (a = x, y, 0(z)), in short,

$$\mathcal{B}^{(xyz)}: (b^{x,-1}, b^{x,0}, b^{x,1}, b^{y,-1}, b^{y,0}, b^{y,1}, c^{0,-1}, c^{0,0}, c^{0,1}, B^{x,0}, B^{y,0}, C^{0,0}). \tag{17}$$

For the rovibrational computations, we transform all quantities from the Cartesian to the spherical representation, in which the electronic wave functions are labeled as $\varphi_n^{\Lambda,\Sigma}$, in short,

$$\mathcal{B}^{(-1,0,1)}: (b^{-1,-1}, b^{-1,0}, b^{-1,1}, b^{+1,-1}, b^{1,0}, b^{1,1}, c^{0,-1}, c^{0,0}, c^{0,1}, B^{+,0}, B^{-,0}, C^{0,0})$$
(18)

with the spherical representation for the Π states (b and B) constructed as $\Pi^{\pm,M_S}=\frac{1}{\sqrt{2}}\left[\Pi^{x,M_S}+i\Pi^{y,M_S}\right]$. Further calculations are collected in the supplementary material. The non-vanishing relativistic (QED) spin-dependent matrix elements (all $\Delta\Omega = 0$) and non-adiabatic ($\Delta \Lambda = \pm 1$; $\Delta \Lambda = 0$ not relevant for the present system) coupling matrix elements used in the coupled equations are collected in Tables S7 and S8.

The coupled radial equations, Eqs. (12) or (14), are solved using the discrete variable representation (DVR) constructed with $L_n^{(\alpha)}$ Laguerre polynomials ($\alpha = 2$), similarly to Refs. 10 and 11 (see also Ref. 60). At the end of the rovibrational and rovibronic computations, we retain the states, for comparison with experiment, that are totally symmetric under the exchange of the two ⁴He²⁺ nuclei (spin-0 bosons).⁵²

First of all, we aim to assess the accuracy of the "absolute" position of the b and c PECs, referenced to the more accurate a-state results.⁴¹ Reference 22 informs us about measured c-a rovibronic intervals, and comparison shows that the cv'N' - avN = c00 - a00electronic-vibrational energy interval differs from the experimental (effective Hamiltonian) data by -2.0 cm⁻¹. The a-PEC⁴¹ is converged to ~0.7 cm⁻¹ (upper bound, and with further variational optimization, this error was already reduced to 0.3 cm⁻¹ in Ref. 41) at $\rho = 2$ bohrs. Hence, the c-a electronic excitation energy error is dominated by the variational convergence error of the c-state electronic energy near equilibrium; the c electronic energy was estimated to be too high by $\sim 10 \ \mu E_h \sim 2 \ \text{cm}^{-1}$, according to the estimated convergence of the c electronic energy (Table S1, supplementary material). Regarding the b state, comparison with the experimental (fine-structure resolved) b-a transitions²³ shows that the computational result is too large by ≈5 cm⁻¹ (Table I), which is dominated by the convergence error of the b-state electronic energy. Indeed, the b ${}^{3}\Pi_{g}$ electronic energy was estimated to be 20–25 μE_{h} too high at $\rho = 2$ bohrs (variational upper bound), which is ≈ 5 cm⁻¹ and in agreement with experiment-theory deviation in the electronic excitation energy. [According to Table S1, the b-state electronic energy obtained with the $N_{\rm b}$ = 1000 basis set, which was used for the PEC generation, has already been improved (lowered) by 9.5 $\mu E_{\rm h}$ $\approx 2.1 \text{ cm}^{-1} \text{ using } N_{\rm b} = 1500 \text{ basis functions. This value can be used}$ to correct the computed rovibronic b-a excitation energies in Table I according to the footnote a of the table.] Both the b and c BO electronic energies can be better converged (with more computing time), if necessary. We expect the rovibrational and fine-structure intervals to be more accurate than the electronic excitation energies, since the approximately homogeneous local error of the PEC largely cancels in the rovibrational (and fine-structure) intervals.

Regarding the rovibronic structure of the c state, we use the rovibrational energy intervals from the experimental work reported in Ref. 24 for comparison. Reference 24 also reports the lifetime of v = 4 and 5 vibrationally excited states. In this work, we compute bound rovibrational states, and the positions of long-lived resonances (relevant for v = 4) were first estimated using the stabilization method.⁶¹ Converging resonance positions and widths, necessary for v = 5 states (and v = 4, N > 10), were incorporated into our rovibronic approach using complex absorbing potentials

TABLE I. Example b–a transition energies, $\tilde{v}_{v_b N_b}^{J_b,b} - \tilde{v}_{v_a N_a}^{J_a,a}$, and rotational–fine-structure intervals, \tilde{f} , computed in this work and compared with experimental values.²³ The $\delta \tilde{v}$ and $\delta \tilde{f}$ experiment–theory deviations are also shown. All values are in cm⁻¹. The levels with v and v are labeled as $v_a N_a$ and $v_b N_b$. The computed a-state energy levels are taken from Ref. 41.

		Expt. ²³		This wo	ork		
$J_{\rm b}$	$J_{\rm a}$	$ ilde{v}_{v_{\mathrm{b}}N_{\mathrm{b}}}^{J_{\mathrm{b}},\mathrm{b}}- ilde{v}_{v_{\mathrm{a}}N_{\mathrm{a}}}^{J,\mathrm{a}}$	$ ilde{ ilde{f}}$	$ ilde{v}_{v_{\mathrm{b}}N_{\mathrm{b}}}^{J_{\mathrm{b}},\mathrm{b}}- ilde{v}_{v_{\mathrm{a}}N_{\mathrm{a}}}^{J_{\mathrm{a}},\mathrm{a}}$	$ ilde{f}$	$\delta ilde{v}^{ m a}$	$\delta ilde{f}$
		Electro		acture transitions (: b01 ← a01 (Q bra			
1	0	4767.4957	0.4049	4772.4570	0.4108	-4.9613	-0.0059
1	1	4767.9006		4772.8678		-4.9672	
2	2	4767.5639	0.3367	4772.4684	0.3994	-4.9045	-0.0627^{b}
			$N_{\rm a}=N_{\rm b}=3$: b03 ← a03 (Q bra	anch):		
2	2	4765.0302	0.2992	4770.0135	0.2982	-4.9833	0.0010
3	3	4765.3294		4770.3117		-4.9823	
4	4	4764.9907	0.3387	4769.9728	0.3389	-4.9821	-0.0002
			$N_a = N_b = 5$: b05 ← a05 (Q bra	anch):		
4	4	4760.4957	0.2996	4765.5038	0.3001	-5.0081	-0.0005
5	5	4760.7953		4765.8039		-5.0086	
6	6	4760.4690	0.3263	4765.4776	0.3264	-5.0086	-0.0001
		N	$V_{\rm a} = N_{\rm b} = 21$:	b0 21 ← a0 21 (Q l	branch):		
20	20	4658.1491	0.3035	4663.7665	0.3017	-5.6174	0.0018
21	21	4658.4526		4664.0682		-5.6156	
22	22	4658.1491	0.3035	4663.7597	0.3085	-5.6106	-0.0050
				e-structure transit		, = 0):	
		N	$I_{\rm b} = 2 \leftarrow N_{\rm a} =$: 1: b02 ← a01 (R l	oranch):		
1	0	4797.0112	-0.2578	4801.9858	-0.2607	-4.9746	0.0029
2	1	4796.7534		4801.7251		-4.9717	
3	2	4796.7700	-0.0166	4801.7432	-0.0181	-4.9732	0.0015
				brational–fine-structure $N_b = 3: b13 \leftarrow a0$			
2	2	4731.9190	0.2915	4737.1109	0.2947	-5.1919	-0.0032
3	3	4732.2105		4737.4055		-5.1950	
4	4	4731.8784	0.3321	4737.0704	0.3351	-5.1920	-0.0030

^aBy further extension (N_b = 1500) and optimization of the b-state fECG basis set (ρ = 2 bohrs; Table S1), the electronic energy is already lowered (variationally) by 2.1 cm⁻¹ (Table S1), which can be used as a correction, $\vec{v}_{vN}^{l,b} - \vec{v}_{vN}^{l,a} - 2.1$ cm⁻¹ and $\delta \vec{v}$ + 2.1 cm⁻¹(≈ −2.9 cm⁻¹).

(CAP)⁶² (alternatively, the complex coordinate rotation technique could also be used).⁶³ Both options require repeated computations, and CAP computations were performed with the finalized and validated rovibronic description of the bc bound-state level structure [Fig. 2(c)].

Figure 2 shows the deviation of experiment and our computations using three different c rovibrational (rovibronic) models. Figure 2(a) shows the result of a single c-state model: it includes all

PEC corrections and the vibrational mass correction in the vibrational kinetic energy, but using the nuclear mass for rotations [i.e., without any rotational mass correction, which would be singular (and undefined) due to the crossing with the b state]. In this single c-state model, highly rotationally excited states exhibit large deviations from experiment, up from 10 to 15 cm⁻¹. Figure 2(b) showcases the bc coupled model, which includes the bc non-adiabatic coupling, all PEC corrections, and the vibrational mass corrections

^bPerhaps a misprint in Ref. 23 (4767.5639 vs. 4767.5039)?

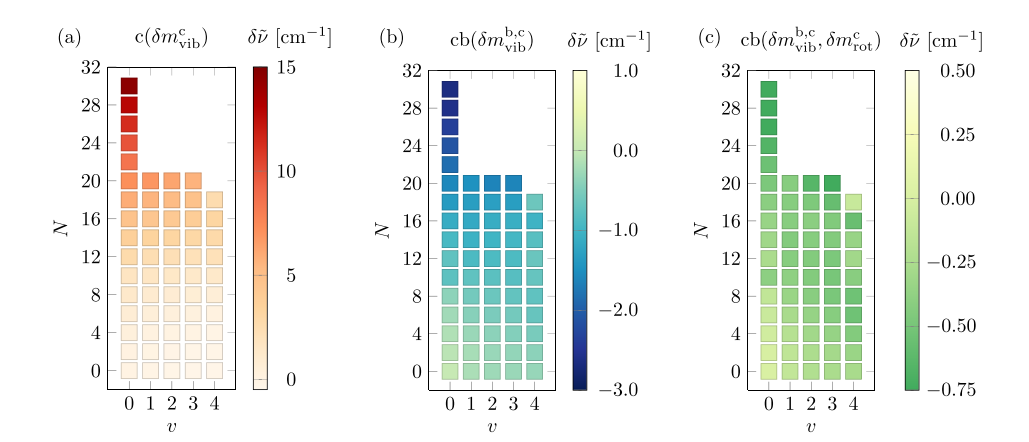


FIG. 2. [(a)–(c)] Rovibrational intervals for c $^3\Sigma_{\rm g}^+$ He₂, cvN-c00 measured from the c00 level (with N=0 and v=0). Deviation of experiment ("Expt."; Ref. 24) and computation ("Comp."; this work), $\delta \bar{v} = \bar{v}_{\rm Exp.} - \bar{v}_{\rm Comp.}$, with three different theoretical models. c($\delta m_{\rm vib}^{\rm b}$): single c-state description with the vibrational mass correction; cb($\delta m_{\rm vib}^{\rm b,c}$): coupled bc description with the vibrational mass corrections; c($\delta m_{\rm vib}^{\rm b,c}$) same as (b) with the rotational mass correction for the c state (please see also the text). In each case, all PEC corrections were included.

for both the b and c states. The high-N rotational angular momentum states deviate from experiment by up to -3 cm^{-1} , which is (in absolute value) by a factor of 5 smaller than the single c-state result. Figure 2(c) shows pilot results from the same bc coupled model, but appended with the c-state rotational mass corrections, which can be rigorously defined for the coupled bc subspace, but the evaluation of the reduced resolvent requires projecting out the active b electronic state contributions. 44 The computation of the c rotational mass corrections assumes an auxiliary basis set of ${}^3\Pi_g$ symmetry (the same as for b) to represent the reduced (i.e., without bc contributions) resolvent, Eq. (10). Including this c-state rotational mass correction in the bc coupled computation reduces the experiment-theory deviations for high-N states by an additional factor of 3, to less than 1 cm⁻¹, which is clearly an improvement (by an order of magnitude) over the 10-15 cm⁻¹ deviation of Fig. 2(a). At the same time, by comparison with the spectacularly accurate ($\sim 0.001 \text{ cm}^{-1}$) a-state rotational intervals, 41 we may wonder what is missing here. First, the auxiliary basis set used in the c rotational mass correction should be optimized more tightly (currently limited by technical difficulties for projecting out the b state). Furthermore, the b state also has a rotational mass correction, and the non-adiabatic mass (kinetic) energy correction has (b-c) off-diagonal terms, 44 which must also be considered. All the missing technical, computational, and formal relations will be elaborated in future work.

Regarding the fine structure of the c-state rovibronic levels, Table II reports fine-structure splittings for selected vibrational states. Since no well-resolved experimental data are currently available, we compare four theoretical models to gain a better understanding of the role of the different contributions. All cases include all PEC corrections and non-adiabatic couplings (in multi-state cases). The currently most complete treatment, labeled as bcBC(rQ), includes all 12 electronic-spin states of the b, c, B, and C electronic states (Tables S6 and S7) coupled by relativistic QED (rQ) interactions. The second most comprehensive model, bc(rQ), includes all nine electron-spin states of the b and c electronic states, and they are coupled by rQ couplings. The bcBC(rQ)-bc(rQ) deviation is (less than) 100 kHz, which is a surprisingly small effect, if we note that the b-B, b-C, and c-B relativistic (QED) couplings (Fig. 1) are comparable to those of the b-b and b-c states. The important difference is that the b-c states are coupled non-adiabatically, whereas the triplet-singlet (bc-BC) states are not (for their different electron spins). The non-adiabatic coupling seems to "enhance" the effect of the relativistic couplings. It is interesting to compare the bc(rQ) and the bc(r) results, the latter including only the relativistic couplings but neglecting the QED corrections of the couplings (from the anomalous magnetic moment of the electron), which has a "large" 2–3 MHz effect (similar to the a-state fine structure⁴¹). Interestingly, the QED effect on the bc magnetic couplings is larger than any magnetic couplings with the BC states. Finally, a single c-state computation (by neglecting any non-adiabatic or relativistic coupling with the b states), but still including the relativistic QED zero-field

TABLE II. Computed c fine structure splittings, $\bar{v}_{N\pm 1} - \bar{v}_N$ in cm⁻¹ with the fully coupled b-c-B-C (bcBC) rovibronic model including non-adiabatic, relativistic (r), and QED couplings (Q). Deviation of the (± 1) fine structure components, $\delta v^{\pm 1}$ in MHz, from this bcBC(rQ) model obtained with bc(rQ): coupled b-c model with non-adiabatic, relativistic, and QED couplings; bc(r): the coupled b-c model with non-adiabatic and relativistic couplings; and c(rQ): the single c-state model with relativistic and QED zero-field splitting.

	bcBC	bc(rQ)		bc(r)		c(rQ)		
N	$\overline{\tilde{v}_{N-1} - \tilde{v}_N}$	$\tilde{v}_{N+1} - \tilde{v}_N$	δv^{-1}	δv^{+1}	δv^{-1}	δv^{+1}	δv^{-1}	δv^{+1}
			c , <i>v</i>	= 0:				
0		0.020 234		-0.1		1.3		0
2	0.039422	0.026643	-0.1	-0.1	2.7	1.7	-34	18
4	0.033 102	0.028839	-0.1	-0.1	2.3	1.8	-50	37
6	0.030 957	0.030212	-0.1	-0.1	2.2	1.9	-68	55
8	0.029659	0.031 288	-0.1	-0.1	2.1	1.9	-85	74
10	0.028 681	0.032 227	-0.1	-0.1	2.1	2.0	-103	93

c, v = 1, 2, and 3: see the supplementary material

c, <i>v</i> = 4:									
0		0.022 045		-0.1		1.5		0	
2	0.042891	0.029 123	-0.2	-0.1	2.9	1.9	-39	23	
4	0.035942	0.031597	-0.2	-0.1	2.4	2.0	-59	45	
6	0.033546	0.033185	-0.2	-0.1	2.3	2.1	-80	68	
8	0.032072	0.034461	-0.2	0.0	2.2	2.2	-102	91	
10	0.030948	0.035600	-0.2	0.0	2.2	2.2	-123	115	

splitting (within the c $^3\Sigma_g^+$ electron spin subspace) has a significant, 30–120 MHz, effect compared to our currently most comprehensive bcBC(rQ) [or almost equally good bc(rQ)] model.

Finally, we report b-a electronic-rotational-vibrational-finestructure transition energies (Table I) obtained from bc(rQ) coupled computations. For a direct, line-by-line comparison with the experimental b-a transitions, we take the (highly accurate) a-state rovibrational-fine-structure energy levels from Ref. 41. The couplings with the B-C PECs were not included in these results, because they have a negligibly small effect (see also the c-state fine structure analysis, Table II). By inspecting Table I, we can assess the accuracy of the b representation at different scales: electronic, vibrational, rotational, and electron spin (fine structure). As pointed out earlier in this work, the b PEC is by ~5 cm⁻¹ too high in energy (out of which 2.1 cm⁻¹ is already confirmed in a larger-basis, currently single $\rho = 2$ bohrs point computation, Table S1). The first vibrational fundamental is accurate to 0.2 cm⁻¹. High-N (up to N = 21 is available from experiment) rotationally excited states are less accurately described, transitions to N = 21 b rotational states are by ~ 0.6 cm⁻¹ less accurate than to N = 1 (again, we emphasize that the a-state rovibrational levels are much more accurate,41 so their theoretical-computational uncertainty is negligible in the present analysis). For a more accurate computation of the b-state rotational excitations, in a bc coupled model, it will be necessary to compute the rotational mass correction of the b state (and of the bc off-diagonal terms); nevertheless, the explicit coupling with the c-state ensures that the deviation is not larger. For the b-state rotational mass correction, auxiliary basis sets of $^3\Sigma_{\rm g}^+$ and $^3\Delta_{\rm g}$ symmetries must be optimized, 45 but the c-state contribution must be projected out, since it is already explicitly coupled with the b state. So, the largest rotational contribution is already accounted for by the explicit bc non-adiabatic coupling. The \tilde{f} fine-structure splittings are in excellent agreement with the experimental data; their deviation from the experimental value is $\delta \tilde{f} \approx 0.001 - 0.003 \text{ cm}^{-1}$, which matches the experimental resolution of Ref. 23.

In summary, we have developed a high-precision rovibronic-relativistic-QED model of the b-c electronic states of the triplet helium dimer. The computed results significantly improve upon earlier work: they account for the electronic, vibrational, rotational, and fine-structure components of the rovibronic spectrum in quantitative agreement with the available experimental data. As a result, we believe that this rovibronic-electron-spin ab initio model can aid ongoing and future experimental work on this simple diatomic system, which exhibits rich magnetic properties. During the introduction of the formalism and the analysis of the computed results, several directions for future improvements were identified, including better convergence of the PECs, non-adiabatic relativistic couplings, b-state rotational mass corrections, spin-rotation coupling computation, and consideration of further electronic states. Priority will be given to the most experimentally useful directions. In the meantime, we are also working on a control program that organizes the several separate or consecutive QUANTEN computing jobs for converging the electronic energy, computing the PEC and all corrections and couplings at the PEC points. Therefore, within the theoretical framework presented in this paper, (even) more accurate and larger-scale computations can be conducted in the future.

The supplementary material includes (a) further theoretical, computational, and convergence details; (b) data points for the PECs and correction and coupling curves are deposited, whose applications are demonstrated in Wolfram Mathematica notebook files; and (c) rovibrational and fine structure energy lists for the b and c electronic states.

We thank the European Research Council (Grant No. 851421) and the Momentum Program of the Hungarian Academy of Sciences (Grant No. LP2024-15/2024) for their financial support. P.J. acknowledges the support of the János Bolyai Research Scholarship of the Hungarian Academy of Sciences (Grant No. BO/285/22). We thank DKF for access to the Komondor HPC facility. This paper is dedicated to John Stanton's memory. We thank John for drawing our attention to the double- and triple-augmented Dunning basis sets.

AUTHOR DECLARATIONS

Conflict of Interest

The authors have no conflicts to disclose.

Author Contributions

Balázs Rácsai: Data curation (equal); Formal analysis (equal); Investigation (equal); Methodology (equal); Software (equal); Writing – original draft (equal); Writing – review & editing (equal). Péter Jeszenszki: Data curation (equal); Funding acquisition (supporting); Software (equal); Writing – review & editing (supporting). Ádám Margócsy: Data curation (equal); Investigation (equal); Methodology (supporting); Writing – original draft (supporting); Writing – review & editing (supporting). Edit Mátyus: Conceptualization (lead); Funding acquisition (lead); Investigation (equal); Methodology (equal); Software (equal); Supervision (lead); Visualization (lead); Writing – original draft (lead); Writing – review & editing (lead).

DATA AVAILABILITY

The data that support the findings of this study are available within the article and its supplementary material.

REFERENCES

- ¹W. Cencek, M. Przybytek, J. Komasa, J. B. Mehl, B. Jeziorski, and K. Szalewicz, "Effects of adiabatic, relativistic, and quantum electrodynamics interactions on the pair potential and thermophysical properties of helium," J. Chem. Phys. 136, 224303 (2012).
- ²P. Jansen, L. Semeria, and F. Merkt, "High-resolution spectroscopy of He⁺₂ using Rydberg-series extrapolation and Zeeman-decelerated supersonic beams of metastable He₂," J. Mol. Spectrosc. **322**, 9 (2016).
- ³L. Semeria, P. Jansen, G. Clausen, J. A. Agner, H. Schmutz, and F. Merkt, "Molecular-beam resonance method with Zeeman-decelerated samples: Application to metastable helium molecules," Phys. Rev. A 98, 062518 (2018).
- ⁴L. Semeria, P. Jansen, G.-M. Camenisch, F. Mellini, H. Schmutz, and F. Merkt, "Precision measurements in few-electron molecules: The ionization energy of metastable ⁴He₂ and the first rotational interval of ⁴He⁺₂," Phys. Rev. Lett. **124**, 213001 (2020).
- ⁵L. Verdegay, B. Zeng, D. Y. Knapp, J. C. Roth, and M. Beyer, "Laser cooling Rydberg molecules A detailed study of the helium dimer," arXiv:2505.14798 (2025)

- 6 L. Semeria, P. Jansen, and F. Merkt, "Precision measurement of the rotational energy-level structure of the three-electron molecule He_2^+ ," J. Chem. Phys. 145, 204301 (2016).
- ⁷P. Jansen, L. Semeria, and F. Merkt, "Fundamental vibration frequency and rotational structure of the first excited vibrational level of the molecular helium ion (He⁺₂)," J. Chem. Phys. **149**, 154302 (2018).
- 8 P. Jansen, L. Semeria, and F. Merkt, "Determination of the spin-rotation fine structure of He₂+," Phys. Rev. Lett. **120**, 043001 (2018).
- 9 W.-C. Tung, M. Pavanello, and L. Adamowicz, "Very accurate potential energy curve of the He_2^+ ion," J. Chem. Phys. **136**, 104309 (2012).
- ¹⁰E. Mátyus, "Non-adiabatic mass-correction functions and rovibrational states of ${}^4\text{He}_2^+$ (X ${}^2\Sigma_u^+$)," J. Chem. Phys. **149**, 194112 (2018).
- ¹¹D. Ferenc, V. I. Korobov, and E. Mátyus, "Nonadiabatic, relativistic, and leading-order QED corrections for rovibrational intervals of ${}^4\text{He}_2^+$ (X ${}^2\Sigma_u^+$)," Phys. Rev. Lett. **125**, 213001 (2020).
- $^{12}\text{E.}$ Mátyus and Á. Margócsy, "Rovibrational computations for He_2^+ X+ Σ_u^+ including non-adiabatic, relativistic and QED corrections," arXiv:2506.19120 (2025).
- M. Beyer, N. Hölsch, J. Hussels, C.-F. Cheng, E. J. Salumbides, K. S. E. Eikema, W. Ubachs, C. Jungen, and F. Merkt, "Determination of the interval between the ground states of para- and ortho-H₂," Phys. Rev. Lett. 123, 163002 (2019).
 M. Puchalski, J. Komasa, P. Czachorowski, and K. Pachucki, "Nonadiabatic
- ¹⁴M. Puchalski, J. Komasa, P. Czachorowski, and K. Pachucki, "Nonadiabatic QED correction to the dissociation energy of the hydrogen molecule," Phys. Rev. Lett. 122, 103003 (2019).
- ¹⁵F. M. J. Cozijn, M. L. Diouf, and W. Ubachs, "Lamb dip of a quadrupole transition in H₂," Phys. Rev. Lett. **131**, 073001 (2023).
- ¹⁶K. Pachucki and J. Komasa, "Relativistic correction from the four-body nonadiabatic exponential wave function," J. Chem. Theory Comput. 20, 8644 (2024).
- ¹⁷S. Xu, A. Lu, X. Zhong, Y. Guo, and J. Shi, "Ab initio investigation of potential energy curves of He₂, He₂⁺, and extrapolation by the machine learning method," Int. J. Quantum Chem. **124**, e27367 (2024).
- ¹⁸M. L. Ginter, "Spectrum and structure of the He₂ molecule. I. Characterization of the states associated with the UAO's $3\rho\sigma$ and 2s," J. Chem. Phys. **42**, 561–568 (1965).
- ¹⁹ M. L. Ginter, "The spectrum and structure of the He₂ molecule: Part III. Characterization of the triplet states associated with the UAO's 3s and $2\rho\sigma$," J. Mol. Spectrosc. **18**, 321–343 (1965).
- ²⁰ M. L. Ginter and R. Battino, "Potential-energy curves for the He₂ molecule," J. Chem. Phys. **52**, 4469–4474 (1970).
- ²¹D. S. Ginter and M. L. Ginter, "The spectrum and structure of the He₂ molecule multichannel quantum defect analyses of the triplet levels associated with $(1\sigma_g)^2(1\sigma_u)np\lambda$," J. Mol. Spectrosc. **82**, 152 (1980).
- ²²C. Focsa, P. F. Bernath, and R. Colin, "The low-lying states of He₂," J. Mol. Spectrosc. 191, 209 (1998).
- 23 S. A. Rogers, C. R. Brazier, P. F. Bernath, and J. W. Brault, "Fourier transform emission spectroscopy of the $b^3\Pi_g$ - $a^3\Sigma_u^+$ transition of He₂," Mol. Phys. **63**(5), 901 (1988).
- 24 D. C. Lorents, S. Keiding, and N. Bjerre, "Barrier tunneling in the He₂ $c^3\Sigma_g^+$ state," J. Chem. Phys. **90**, 3096 (1989).
- ²⁵C. M. Brown and M. L. Ginter, "Spectrum and structure of the He₂ molecule VI. Characterization of the states associated with the UAO's $3p\pi$ and 2s," J. Mol. Spectrosc. **40**, 302 (1971).
- 26 B. Brutschy and H. Haberland, "Long-range helium excimer potentials (A, $C^{1}\Sigma_{u,g}^{+}$, and a, $c^{3}\Sigma_{u,g}^{+}$) from high-resolution differential cross sections for He(21 S, 23 S)+He," Phys. Rev. A 19, 2232–2248 (1979).
- ²⁷ M. Kristensen and N. Bjerre, "Fine structure of the lowest triplet states in He₂," J. Chem. Phys. **93**, 983 (1990).
- ²⁸I. Hazell, A. Norregaard, and N. Bjerre, "Highly excited rotational and vibrational levels of the lowest triplet states of He₂: Level positions and fine structure," J. Mol. Spectrosc. **172**, 135 (1995).
- ²⁹R. A. Buckingham and A. Dalgarno, "The interaction of normal and metastable helium atoms," Proc. R. Soc. A 213, 327–349 (1952).

- ³⁰R. S. Mulliken, "Rare-gas and hydrogen molecule electronic states, noncrossing rule, and recombination of electrons with rare-gas and hydrogen ions," Phys. Rev. **136**, A962–A965 (1964).
- ³¹S. L. Guberman and W. A. Goddard, "Nature of the excited states of He₂," Phys. Rev. A 12, 1203–1221 (1975).
- 32 J. Wasilewski, V. Staemmler, and R. Jaquet, "CEPA calculations on open-shell molecules. III. potential curves for the six lowest excited states of He $_2$ in the vicinity of their equilibrium distances," Theor. Chim. Acta 59 , 517–526 (1981).
- ³³K. K. Sunil, J. Lin, H. Siddiqui, P. E. Siska, K. D. Jordan, and R. Shepard, "Theoretical investigation of the a ${}^3\Sigma_{\rm u}^+$, A ${}^1\Sigma_{\rm u}^+$, c ${}^3\Sigma_{\rm g}^+$, and C ${}^1\Sigma_{\rm g}^+$ potential energy curves of He₂ and of He*(2 1S , 2 3S)+He scattering," J. Chem. Phys. **78**, 6190 (1983).
- ³⁴C. F. Chabalowski, J. O. Jensen, D. R. Yarkony, and B. H. Lengsfield, "Theoretical study of the radiative lifetime for the spin-forbidden transition $a^3\Sigma_u^+ \to X^1\Sigma_g^+$ in He₂," J. Chem. Phys. **90**, 2504 (1989).
- ³⁵D. R. Yarkony, "On the quenching of helium 2³S: Potential energy curves for, and nonadiabatic, relativistic, and radiative couplings between, the a $^3\Sigma_{\rm u}^+$, A $^1\Sigma_{\rm u}^+$, b $^3\Pi_{\rm g}$, B $^1\Pi_{\rm g}$, c $^3\Sigma_{\rm g}^+$, and C $^1\Sigma_{\rm g}^+$ states of He₂," J. Chem. Phys. **90**, 7164 (1989).
- ³⁶B. Minaev, "Fine structure and radiative lifetime of the low-lying triplet states of the helium excimer," Phys. Chem. Chem. Phys. **5**, 2314 (2003).
- ³⁷N. Bjerre, A. O. Mitrushenkov, P. Palmieri, and P. Rosmus, "Spin-orbit and spin-spin couplings in He₂ and He₇", Theor. Chem. Acc. **100**, 51 (1998).
- ³⁸P. Nijjar, A. I. Krylov, O. V. Prezhdo, A. F. Vilesov, and C. Wittig, "Triplet excitons in small helium clusters," J. Phys. Chem. A 123, 6113–6122 (2019).
- ³⁹M. D. E. Epée, O. Motapon, K. Chakrabarti, and J. Tennyson, "Theoretical investigation of Rydberg states of He₂ using the *R*-matrix method," Mol. Phys. **122**, e2295013 (2024).
- ⁴⁰M. Pavanello, M. Cafiero, S. Bubin, and L. Adamowicz, "Accurate Born–Oppenheimer calculations of the low–lying $c^3 \Sigma_g^+$ and $a^3 \Sigma_u^+$ excited states of helium dimer," Int. J. Quantum Chem. 108, 2291 (2008).
- ⁴¹Á. Margócsy, B. Rácsai, P. Jeszenszki, and E. Mátyus, "Rovibrational computations for the He₂ a $^3\Sigma_u^+$ state including non-adiabatic, relativistic, and QED corrections," arXiv:2506.19116 (2025).
- ⁴²P. Jeszenszki, P. Hollósy, Á. Margócsy, and E. Mátyus, "Spin-dependent terms of the Breit-Pauli Hamiltonian evaluated with explicitly correlated Gaussian basis set for molecular computations," arXiv:2506.19131 (2025).
- ⁴³H. Lefebvre-Brion and R. W. Field, *The Spectra and Dynamics of Diatomic Molecules* (Academic Press, 2004).
- ⁴⁴E. Mátyus and Teufel, "Effective non-adiabatic Hamiltonians for the quantum nuclear motion over coupled electronic states," J. Chem. Phys. 151, 014113 (2019).
- 45 E. Mátyus and D. Ferenc, "Vibronic mass computation for the EF–GK–HH $^{1}\Sigma_{g}^{+}$ manifold of molecular hydrogen," Mol. Phys. **120**, e2074905 (2022).
- ⁴⁶D. Ferenc and E. Mátyus, "Non-adiabatic mass correction for excited states of molecular hydrogen: Improvement for the outer-well $H\bar{H}^{-1}\Sigma_g^+$ term values," J. Chem. Phys. **151**, 094101 (2019).
- ⁴⁷B. Rácsai, D. Ferenc, A. Margócsy, and E. Mátyus, "Regularized relativistic corrections for polyelectronic and polyatomic systems with explicitly correlated Gaussians," J. Chem. Phys. 160, 211102 (2024).
- ⁴⁸S. N. Yurchenko, L. Lodi, J. Tennyson, and A. V. Stolyarov, "Duo: A general program for calculating spectra of diatomic molecules," Comput. Phys. Commun. **202**, 262 (2016).
- ⁴⁹P. Quadrelli, K. Dressler, and L. Wolniewicz, "Weak predissociation of the *EF*, GK, and $H^{1}\Sigma_{g}^{+}$ states of the H_{2} molecule by nonadiabatic coupling with the electronic ground state," J. Chem. Phys. **93**, 4958 (1990).
- 50 S. Yu and K. Dressler, "Calculation of rovibronic structures in the lowest nine excited $^1\Sigma_g^+ + ^1\Pi_g + ^1\Delta_g$ states of H₂, D₂, and T₂," J. Chem. Phys. **101**, 7692 (1994).
- ⁵¹ W. Kołos and L. Wolniewicz, "Nonadiabatic theory for diatomic molecules and its application to the hydrogen molecule," Rev. Mod. Phys. 35, 473 (1963).
- ⁵²J. Brown and A. Carrington, Rotational Spectroscopy of Diatomic Molecules (Cambridge University Press, Cambridge, 2003).
- 53Y. Suzuki and K. Varga, Stochastic Variational Approach to Quantum-Mechanical Few-Body Problems (Springer-Verlag, Berlin, 1998).

- ⁵⁴E. Mátyus and M. Reiher, "Molecular structure calculations: A unified quantum mechanical description of electrons and nuclei using explicitly correlated Gaussian functions and the global vector representation," J. Chem. Phys. 137, 024104 (2012).
- $^{55}\rm M.$ J. D. Powell, "The NEWUOA software for unconstrained optimization without derivatives (DAMTP 2004/NA05)," Report No. NA2004/08, 2004.
- ⁵⁶W. Cencek and J. Rychlewski, "Many-electron explicitly correlated Gaussian functions. II. Ground state of the helium molecular ion He⁺₂," J. Chem. Phys. **102**, 2533 (1995).
- ⁵⁷D. Ferenc and E. Mátyus, "Benchmark potential energy curve for collinear H₃," Chem. Phys. Lett. **801**, 139734 (2022).
- ⁵⁸ K. Pachucki, W. Cencek, and J. Komasa, "On the acceleration of the convergence of singular operators in Gaussian basis sets," J. Chem. Phys. **122**, 184101 (2005).
- ⁵⁹ P. Jeszenszki, R. T. Ireland, D. Ferenc, and E. Mátyus, "On the inclusion of cusp effects in expectation values with explicitly correlated Gaussians," Int. J. Quantum Chem. 122, e26819 (2022).
- 60 G. Avila and E. Mátyus, "Toward breaking the curse of dimensionality in (ro)vibrational computations of molecular systems with multiple large-amplitude motions," J. Chem. Phys. **150**, 174107 (2019).
- ⁶¹ A. U. Hazi and H. S. Taylor, "Stabilization method of calculating resonance energies: Model problem," Phys. Rev. A 1, 1109 (1970).
- ⁶²B. Poirier and T. Carrington, Jr., "Semiclassically optimized complex absorbing potentials of polynomial form. I. Pure imaginary case," J. Chem. Phys. 118, 17 (2003).
- ⁶³N. Moiseyev, "Quantum theory of resonances: Calculating energies, widths and cross-sections by complex scaling," Phys. Rep. 302, 212 (1998).